Fire Technology, 53, 1555–1568, 2017

DOI: 10.1007/s10694-017-0647-1

The Wind Effect on the Transport and Burning of Firebrands

Jiayun Song, Naian Liu, Han Li and Linhe Zhang, State Key Laboratory of Fire Science, University of Science and Technology of China, Hefei, 230026 Anhui, People's Republic of China*

Xinyan Huang, Department of Mechanical Engineering, University of California at Berkeley, Berkeley, CA 94720, USA

Received: 29 March 2016/**Accepted:** 6 January 2017

Abstract. Firebrands, controlling spot fires, are often responsible for fast damages in wildland and urban fires. However, the behaviours of firebrands are difficult to predict. In this study, we conduct experiments in a wind tunnel to investigate the effect of wind on the smouldering burning and transport of firebrands. Three different sizes of disc wood particles (weighing about 1 g) are heated to generate smouldering firebrands, and then blown out by a horizontal wind of 5 or 7 m/s. In each experiment the transport distance (in the order of 1 m) and mass loss of firebrands are measured to examine their burning behaviours. For the first time, a bimodal distribution (burning and extinction modals) is observed for small firebrands under certain wind speeds (firebrands of 12-mm diameter and 5-mm thickness under a wind speed of 7 m/s in this work). Both the firebrand transport distance and mass loss in the extinction modal are smaller than those in the burning modal. The heat transfer analysis shows that there is a critical wind speed to quench the firebrand and produce a bimodal distribution, and its value increases with both the particle size and the heating duration. The predicted critical wind speed agrees well with experimental measurements.

Keywords: Spot fire, Smouldering, Extinction, Bimodal distribution, Critical wind speed

1. Introduction

Firebrands are lifted burning embers, often produced in large-scale wildland, urban, and post-earthquake fires. They are responsible for the unpredictably fast damages in many fires such as the Great (urban) Fires of London (1666) and San Francisco (1906) or more recently the wildland fires in Australia and Greece [1, 2]. Firebrands can control and accelerate the fire spread by breaking fire defence lines to ignite surrounding cities, and make the firefighting extremely difficult [3–6]. The discontinuous fire spread led by firebrands is referred to as spotting. It is known that spotting becomes more significant with increasing fire intensity and size, however, the behaviour of spotting is difficult to predict [5]. Therefore, firebrand and

* Correspondence should be addressed to: Naian Liu, E-mail: liunai@ustc.edu.cn

spotting behaviour are critical elements of large-scale wildfires, conflagrations and wildland-urban interface (WUI) fires [7].

The research on firebrand during the past several decades involves three main topics: (1) firebrand generation and release; (2) firebrand lofting and transport; (3) firebrand deposition and subsequent ignition of recipient fuels [8, 9]. Particularly, a large amount of research focused on the firebrand transport. Tarifa et al. [10, 11] pioneered the wind-tunnel experiment on firebrand transport to study the influence of firebrand size, shape, density, type and moisture on the transport distance. They determined the flight paths and lifetimes of burning wooden brands for both uniform ambient horizontal wind and basic vertical or inclined constant-velocity convection column models. Lee and Helman [12] studied the aerodynamic behaviour of spherical firebrands in a turbulent swirling plume and established two empirical correlations for the burning rate. Albini [13] developed a burning-rate model based on the linear relationship between the burning rate and the wind speed, and used it to consider the transport of firebrands by line thermals for wind-driven fires. Woycheese and Pagni [14] determined the maximum propagation distance of combusting disk-shaped brands exposed to the above-mentioned two-distinct-component flow field. Himoto and Tanaka [15], and Koo et al. [3] studied the transport of disk-shaped firebrands using a CFD (computational fluid dynamics) model to predict the plume characteristics. Recently, Manzello and co-workers [16–20] have determined the size and mass distribution of firebrands produced from burning trees and developed an experimental apparatus, known as the NIST Firebrand Generator(NIST Dragon) to simulate the generation and transportation of firebrand in real wildfires. Fernandez-Pello and co-workers [21, 22] developed a numerical model to predict the transport distance for different types of firebrand. Sardoy et al. [23, 24] numerically predicted a bimodal distribution for flaming and smouldering firebrands, and the spacing between the two distributions depended on the char content. Ellis [6, 25] studied in detail the aerodynamic and combustion characteristics of the stringy bark firebrand samples, such as the flaming time, burnout time, terminal velocity, and mass, thanks to experiments made in the CSIRO verticle wind tunnel [26, 27]. Tohidi et al. [28] used the Monte-Carlo simulation of firebrand transport through the velocity field induced by the interaction of a fire plume and the atmospheric boundary layer. More recently, the transport behaviours of firebrand have been incorporated into models for large-scale wildfires [29, 30]. However, to the best of the authors' knowledge, the extinction of a burning firebrand and its interaction with the wind and transport have not been studied experimentally and theoretically. In fact most of previous works focus on numerical simulation without experimental verification.

In this work, a well-controlled wind tunnel experiment is performed to study the smouldering during the generation and transport of disc-shaped firebrands. We quantify the distributions of transport distance and residue mass of firebrands with different sizes to examine their burning behaviours. A simple heat transfer analysis is then proposed to explain the extinction of firebrand and its influence on the distance and mass distributions.

2. Experimental Setup

Figure 1 shows some photos and a schematic diagram of the experimental setup. The test facilities are placed inside a wind tunnel 5 m long, 1.8 m wide and 1.8 m tall (Figure 1a), including the fan, water pan array, and heating device (Figure 1b). The fan of 4 m diameter produces the wind field with wind speeds up to 10 m/s. In this study, two wind speeds are tested, 5 and 7 ($\pm$ 0.3) m/s, which are typical in wildland fires [31, 32] corresponding to Scale 3 and 4 in the Beaufort wind force scale [33]. In pre-experiments we also tried to use a lower wind speed of 3 m/s for test, however it was observed that the particle with 10-mm diameter and 24-mm thickness cannot be thrown out under this wind speed. We also tested a higher wind speed of 9 m/s, under which the particle with 5-mm diameter and 12-mm thickness was thrown beyond the zone of the water pan and so could not be collected.

In experiments, a 30 $\times$ 10 cm^2 quartz heating plate is used to heat wood particles uniformly, and generate firebrands with similar initial burning condition. This heating plate is placed inside the steel shelf which is mobile in the vertical direction and held by an electromagnet during the initial heating process (see Figure 1b). There are 10 densely arranged quartz tubes inside the heating plate, which provides a power of 2 kW. The surface temperature of heating plate is

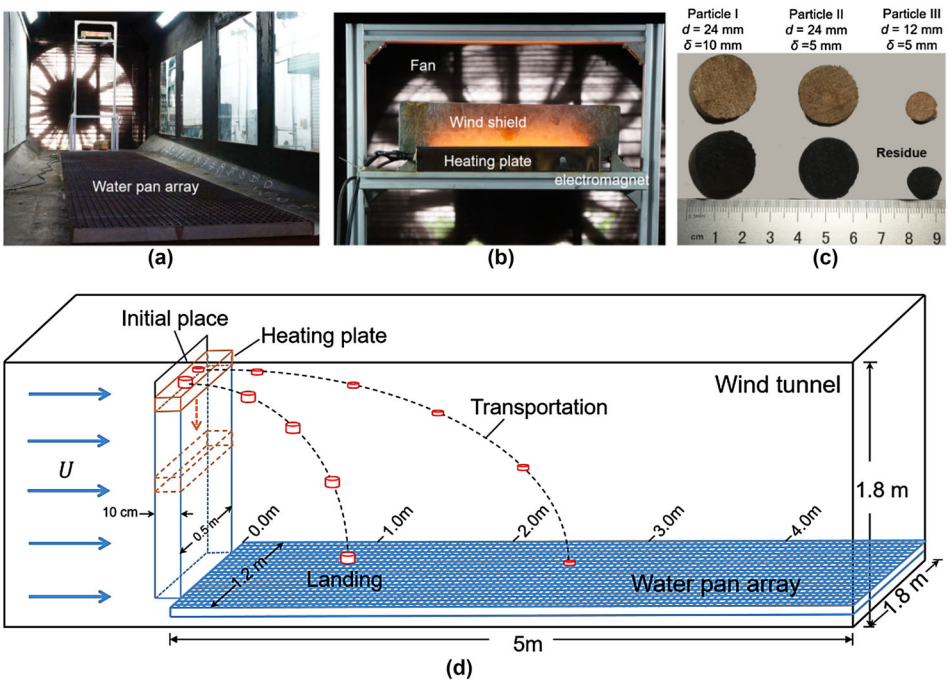

Figure 1. Experimental setup for the generation, transport and landing of firebrands: (a) wind tunnel, (b) heating device, (c) disc-shaped particles, and (d) schematic diagram.

monitored by six 0.5-mm K-type thermocouples with 5 cm spacing, and stabilized at 600 ± 10°C under an ambient temperature of 25 ± 2°C. During heating, wood particles are placed on the heating plate and shielded from the wind. Upon reaching the pre-set heating time, power is turned off both for the heating plate and the electromagnet. Without the holding by the electromagnet, the heating plate and wood particles start to free fall. Meanwhile, wood particles start to be blown out by the horizontal wind, becoming firebrands. In the experiment, no flaming is observed in the wood particles, so the ignition or the burning is purely smouldering.

Disc-shaped firebrands have been widely observed in both structure and wildland fires [18]. In this study, three sizes of disc Eucalyptus wood particles (I–III from large to small) are tested, as shown in Figure 1c. Preliminary experiments show no smouldering if the heating time is below 30 s, and burnout if the heating time exceeds about 4 min. Thus the heating time is set to ensure a robust smouldering ignition while avoiding noticeable change in particle diameter and thickness, as summarized in Table 1. Prior to heating, all particles are dried in the oven at 50°C [34, 35] for 3 h to avoid the influence of the initial moisture, and then their dry masses are measured (m_0). For each run, a fixed number of the same type of particles (see Table 1) are heated at the same time on the hot plate.

In order to measure the transport distance, size and mass of firebrands, an array of 3000 small water pans (5 × 3 cm^2) is placed downstream to collect firebrands. These small pans are able to acquire the precise landing location for each firebrand, and the water is used to quickly extinguish the firebrand to avoid further mass loss. After the experiment, the firebrands in each pan are counted. The firebrands are then filtered from the water and dried in oven at 110°C for 8 h. Then, the dry mass of each firebrand is measured to obtain the distribution (N/N_{tot}) of residue mass.

In order to decouple the influence of wind and heating, two groups of reference tests are conducted. One is to measure the transport distance under the same wind but without heating by hot plate (i.e. unheated particles). The other is to measure the mass right after the same heating process without wind and transport process (i.e. no-transport particles without wind). For each test condition (particle size and wind speed), at least 10 repeating runs are conducted, so hundreds of firebrands are recorded in a distribution.

Table 1
Summary of the Tested Wood Particles and Heating Conditions Under Wind Speeds of 5 and 7 m/s

Particle type	Diameter d (mm)	Thickness δ (mm)	Initial mass m_0 (g)	Heating time t_h (s)	Particle No. (-)
I	24	10	2.45 ± 0.05	120	10
II	24	5	1.25 ± 0.05	90	10
III	12	5	0.34 ± 0.01	60	15

3. Experimental Results

The fire hazard of firebrand is determined by its ignitibility and transport distance. The ignitability is related to its size and burning condition (e.g. flaming, smouldering, and burning duration). The transport distance of firebrand contributes to the wildfire spread and determines the safety distance for preventing spot fires [36]. With the wind, some firebrands may reach farther land to induce new fires, but their ignitability may also be affected by the wind. Therefore, quantifying the interaction among the burning process, transport distance and wind is important to evaluate the fire hazard of firebrands.

Figure 2a, c show the measured distributions (N/N_{tot}) of transport distance for the large-size Particle I (d = 24 mm, δ = 10 mm) under 5 m/s and 7 m/s wind, compared with reference distributions of unheated particles. Table 2 summarizes the measured transport distance and normalized residue mass (m/m_0) for all three heated particles. Compared to unheated particles, heated particles generally fly much farther because of the mass loss during heating and flying. In addition, as the wind speed increases from 5 m/s to 7 m/s, the observed maximum transport (spotting) distance increases from 210 cm to 320 cm, and the modal transport distance increases from 60 cm to 100 cm.

Figure 2b, d show the residue mass distributions of firebrands under 5 m/s and 7 m/s wind speeds, compared with reference distributions of no-transport particles without wind. The measured modal masses are 49% (5 m/s) and 45% (7 m/s), respectively (see Table 2), and they are clearly lower than no-transport particles (72%). In other words, a significant part of wood particle is burnt in transport, and in particular for this large Particle I, the mass lost (23–27%) in transport is similar to 28% (= 1–72%) found in heating. On the other hand, increasing wind speed from 5 m/s to 7 m/s has a minor effect on the mass loss, as compared to the effect on the transport distance shown in Figure 2a, c. Note that for Particle I, the unimodal distribution is observed for both transport distance and residue mass.

Figure 3 shows the measured distributions of transport distance and residue mass for the medium-size Particle II (d = 24 mm, δ = 5 mm). Similar unimodal distributions are found for both transport distance and residue mass. Comparison with the large Particle I (Figure 2) shows that the transport distance increases as the mass reduces by half: for instance under a 5 m/s wind, the modal distance increases from 60 cm to 100 cm and maximum spotting distance increases from 210 cm to 260 cm, as summarized in Table 2. More importantly, as the particle size decreases, the transport and burning become more sensitive to the wind speed change. For example, as the wind speed increases from 5 m/s to 7 m/s, the modal distance increases to 60 m and the mass loss increases to 12%, much larger than the values of 40 m and 4% found for the large Particle I.

Figure 4 shows the measured distributions of transport distance and residue mass for the small-size disc Particle III (d = 12 mm, δ = 5 mm). As the particle size continues to decrease, the transport distance further increases and the residue mass further decreases. Under 5 m/s wind, a unimodal distribution is observed, similar to Particles I and II. However, under 7 m/s wind a bimodal distribution is

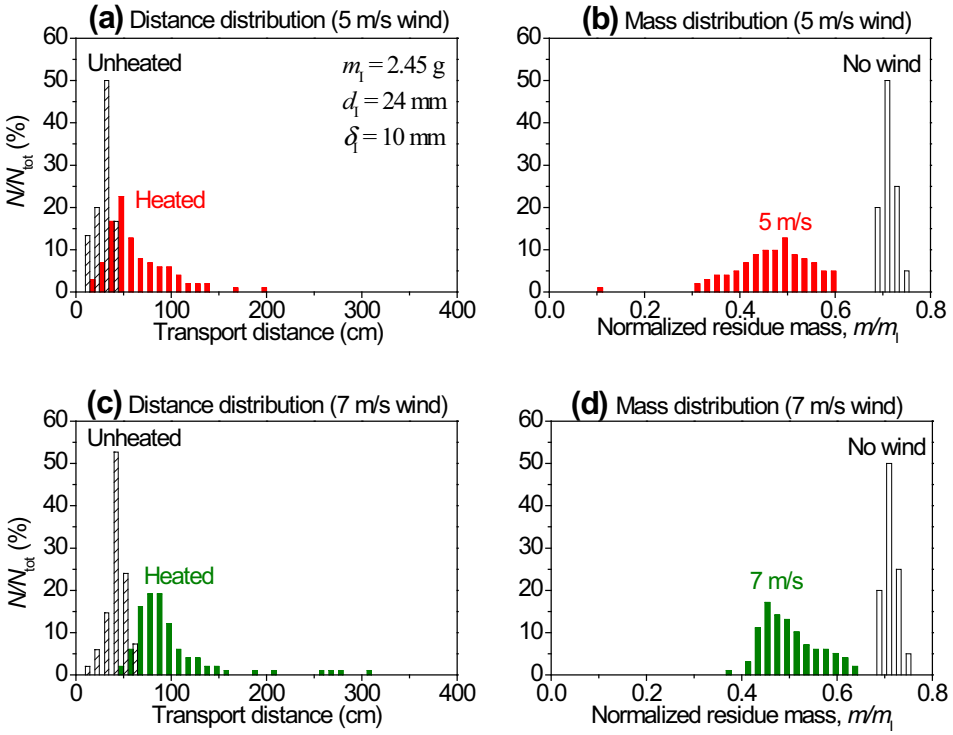

Figure 2. For large-size Particle I (d = 24 mm, δ = 10 mm), distributions of (a) transport distance and (b) residue mass under 5 m/s wind; (c) transport distance and (d) residue mass under 7 m/s wind. The reference distributions for (1) unheated particles and (2) no-transport particles without wind are given.

Table 2
Measured Transport Distance and Residue Mass, and Calculated Critical Wind Speeds, for Three Heated Particles

Disc particle Wind speed	Modal distance $\bar{L}$ (cm)		Max. distance L_{max} (cm)		Normalized modal mass $\bar{m}/m_0$ (%)		Critical wind U^* (m/s)
	5 m/s	7 m/s	5 m/s	7 m/s	5 m/s	7 m/s	
I	60	100	210	320	49	45	5.9
II	100	160	260	360	53	41	14.7
III	120	130/200	360	400	47	57/33	37.7

For small Particle III at 7 m/s wind, values of extinction/burning mode are listed

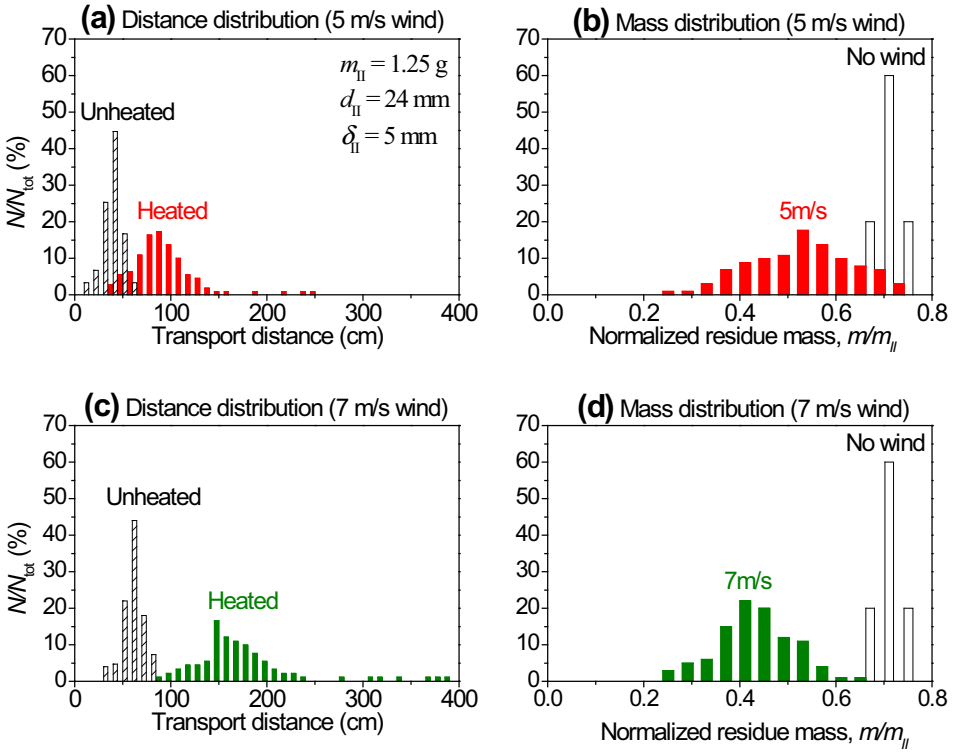

Figure 3. For medium-size Particle II (d = 24 mm, δ = 5 mm), distributions of (a) transport distance and (b) residue mass under 5 m/s wind; (c) transport distance and (d) residue mass under 7 m/s wind. The reference distributions for (1) unheated particles and (2) no-transport particles without wind are given.

found for both transport distance in Figure 4c and residue mass in Figure 4d, different from all other tested cases.

One possible explanation for such bimodal distribution is that as the wind speed increases to a critical value, a significant number of ignited firebrands are quenched by the wind (extinction mode). For the small Particle III, the critical wind speed for the distribution change is between 5 and 7 m/s. Two experimental observations support this explanation: (1) the residue masses of these quenched firebrands remain large, and are close to those no-transport particles which are quenched manually after heating, as seen in Figure 4d; and (2) their transport distances are substantially shorter than those in the burning mode, and close to unheated particles, as seen in Figure 4c.

Moreover, it can be predicted that as the wind speed further increases, (1) the transport distances of both modes will increase; (2) the distance between two modes will increase; (3) the number of firebrands in extinction mode will increase;

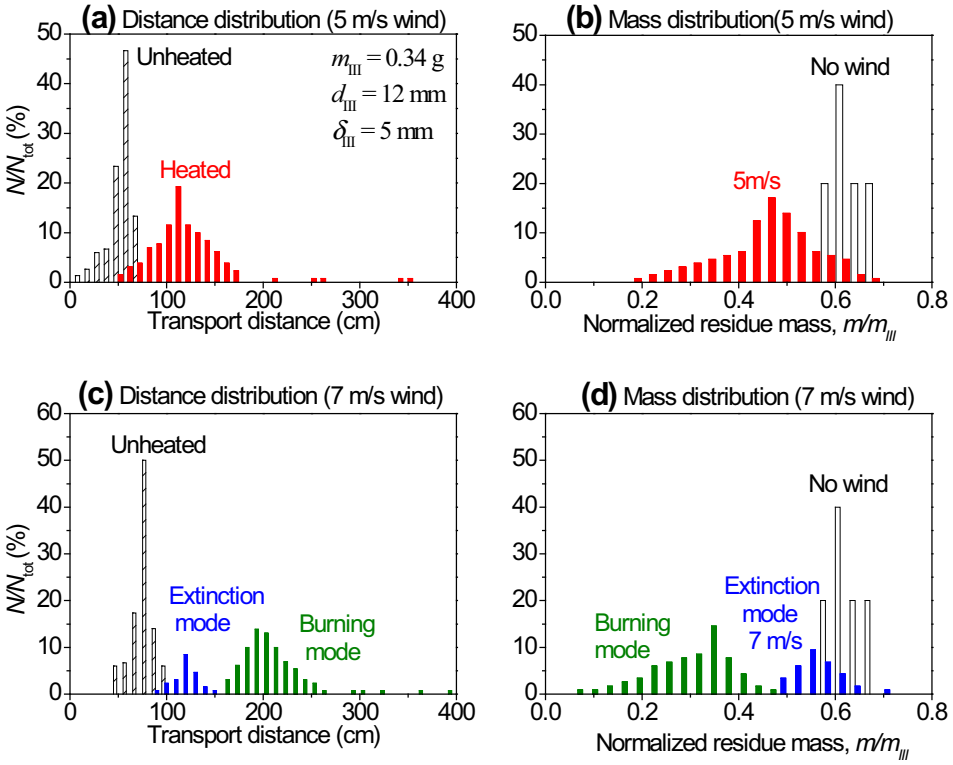

Figure 4. For small-size Particle III (d = 12 mm, δ = 5 mm), distributions of (a) transport distance and (b) residue mass under 5 m/s wind; (c) transport distance and (d) residue mass under 7 m/s wind. The reference distributions for (1) unheated particles and (2) no-transport particles without wind are given.

and (4) the distributions of extinction mode will further move towards both reference experiments.

4. Discussions

In this section, a simplified theoretical analysis is proposed to explain the bimodal distribution for small-size disc Particle III and to predict the critical wind speed for other particles. During transport, wind provides oxygen to support the burning of firebrand (smouldering in the current cases), but at the same time makes the firebrand cool down. As the cooling rate increases with wind speed, the firebrand temperature will decrease and become prone to extinction.

Therefore, the critical wind speed (U^*) appears when the smouldering heating rate ($\dot{Q}_{sm}$) is equal to the wind cooling rate ($\dot{Q}_c$) as

$$\dot{Q}_{sm}(t) = \dot{Q}_c(\Delta U) \tag{1a}$$

where ΔU is the relative speed between firebrand and air. During the transport occurring in the current experimental setup, the cooling rate decreases as ΔU decreases, and the heating rate increases as the burning area increases. Thus, both the maximum cooling rate and the minimum heating rate occur at the beginning of transport: $\Delta U_{max} = U^*$ and $t = t_h$ as

$$\dot{Q}_{sm}(t_h) = \dot{Q}_c(U^*). \tag{1b}$$

In other words, if the particle is not quenched at the beginning of flight, it will keep burning and fly much farther than quenched particles, as observed in Figure 4c. Meanwhile, the distance distribution of quenched particles is close to that of unheated particles.

Note that in this work the wind is assumed to be in horizontal direction with a constant wind speed. In real wildfires, wind changes with time and can be altered by plume, leading to complex relative motion between wind and firebrand, which may cause the maximum relative speed to occur during the flight.

The maximum cooling rate can be estimated by Newton's cooling law as

$$\dot{Q}_c(U^*) = h_c A(T_0 - T_a). \tag{2}$$

where $A = \pi d^2/4$ is the area of the surface in contact with the hot plate; $T_0 = 600°C$ is the particle surface temperature at $z = 0$, same as the temperature of hot plate; $T_a = 25°C$ is the measured ambient temperature; and $h_c = Nu_w \lambda_a / d$ is the convective heat transfer coefficient for cooling. For the cooling of wind, the Nusselt number (Nu_w) is a function of Prandtl number (Pr) and Reynolds number ($Re_d = U^* d/\nu_a$) [22] as

$$Nu_w = 0.42Pr^{0.2} + 0.57Re_d^{1/2}Pr^{1/3} \quad \left(1 < Re_d < 10^4\right) \tag{3}$$

where $\nu_a = 15 \times 10^{-6}$ m^2/s [37] is the air kinematic viscosity; and it is found that $Re_d \sim \mathrm{O}(10^3)$. Therefore, we can estimate that the cooling rate increases with the wind speed as $\dot{Q}_c(U^*) \propto (U^*)^{1/2}$ while decreases with the particle diameter as $\dot{Q}_c(U^*) \propto d^{-1/2}$.

As the wind speed suddenly increases, oxygen supply is assumed to be sufficient for the entire particle. Thus, the minimum heating rate can be estimated as

$$\dot{Q}_{sm}(t_h) = \Delta H_{sm} \dot{\omega} m Y_{sm}(t_h) \tag{4}$$

where ΔH_{sm} is the heat of smouldering for wood; $\dot{\omega}$ is the average rate of exothermic smouldering reaction in wood, for which an average rate of char oxidation between 400°C and 600°C found in thermogravimetric analysis [38] is used (see Table 3); the mass of particle is $m = \rho A \delta$; and $Y_{sm}(t_h)$ is the mass fraction of parti-

Table 3
Physicochemical Properties of the Smouldering Firebrand [40, 41]

ρ (kg/m^3)	λ [40] (W/m–K)	c [40] (J/kg-K)	$\dot{\omega}$ [38] (s^{-1})	ΔH_{sm} [42] (MJ/kg)
650	0.24	1466	1.5×10^{-3}	20

cle in the exothermic smouldering reaction at t_h, which can be approximated as the thickness fraction of particle with temperature higher than 400°C.

The particle temperature profile, $z(T)$, at the end of heating (t_h) can be estimated by a one-dimensional (1D) transient heat conduction equation in the vertical direction (see Figure 5):

$$\rho c \frac{\partial T}{\partial t} = \lambda \frac{\partial^2 T}{\partial z^2}. \tag{5}$$

The change in particle thickness (δ) is negligible as observed in the experiments. The initial and boundary conditions are set based on the heating process on the hot plate:

$$\begin{cases} T(z, t_0) = T_a = 25°\text{C} & (t_0 = 0) \\ T(0, t) = T_0 = 600°\text{C} & (z = 0, 0 < t \le t_h) \\ \lambda \frac{\partial T(\delta, t)}{\partial z} = h_\delta (T_\delta - T_a) & (z = \delta, 0 < t \le t_h) \end{cases} \tag{6}$$

where ρ, c, and λ are the density, specific heat, and thermal conductivity of wood, respectively (see Table 3); and $h_\delta = Nu_g \lambda_a / d$ is the cooling at the top surface ($z = \delta$), dominated by the natural convection as a function of Rayleigh number ($Ra = g\beta(T - T_a)L^3/(v_a \alpha_a)$) [39]:

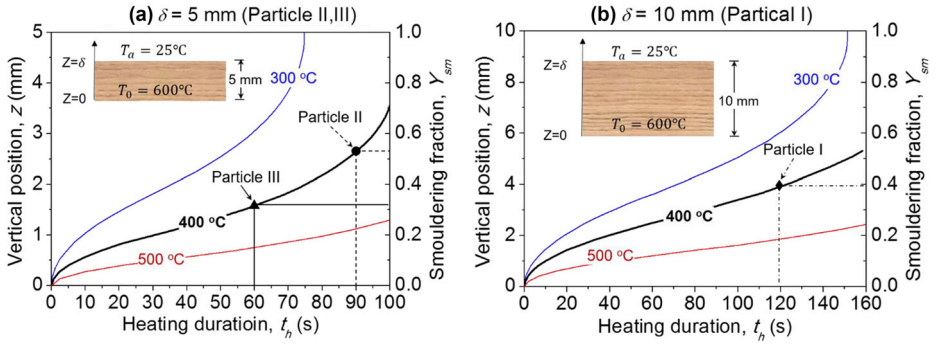

Figure 5. The solved evolution of temperature and fraction of smouldering (Y_{sm}) (a) particles II and III (thickness δ = 5 mm), and (b) particles I (thickness δ = 10 mm).

$$Nu_g = 0.15Ra^{\frac{1}{3}}, \quad \left(10^7 < Ra < 10^{11}\right) \tag{7}$$

where $g = 9.81\ \mathrm{m/s^2}$ is the gravitational acceleration; α_a is the air thermal diffusivity; $L = 0.9d$ is the characteristic length-scale for disc; $\beta = 1/\bar{T}$ is the coefficient of thermal expansion; $\bar{T} = (T + T_a)/2$ is the characteristic temperature; and it is found that $Ra \sim \mathrm{O}(10^9)$. Equation (7) shows that $Nu_\delta \propto d$, so h_δ and the temperature profile are independent of the particle diameter. All particle physicochemical properties are listed in Table 3, and Equation (5) can be solved numerically.

Figure 5 shows the solved evolution of temperature profile and mass fraction of smouldering (Y_{sm}) for (a) Particles II and III (δ = 5 mm thick), and (b) Particles I (δ = 10 mm thick). As the heating duration increases, Y_{sm} and the degree of smouldering increases, resulting in a greater heating rate ($\dot{Q}_{sm}$). Therefore, a larger wind speed is required to cool and extinguish the particle.

The correlation among critical wind speed (U^*), particle thickness (δ), and heating duration (t_h) can be found by solving Equation (1), as presented in Figure 6. As expected, the critical wind speed increases with both the particle thickness and the heating duration. Figure 6a shows that the predicted critical wind speed for Particle III (δ = 5 mm and t_h = 60 s) is U^*_{III} = 5.9 m/s (21 km/h), which is between two experimental wind speeds (5 and 7 m/s). Therefore, the extinction mode could only occur under 7 m/s wind, agreeing with the experimental observation and the measured distributions in Figure 4.

Figure 6b also predicts that for the large 24-mm diameter Particle I (δ = 10 mm and t_h = 120 s) and Particle II (δ = 5 mm and t_h = 90 s), the critical wind speeds are U^*_I = 37.7 m/s (136 km/h, ~ Scale 12) and U^*_{II} = 14.7 m/s (53 km/h, ~ Scale 7), respectively. Field measurements [31, 32] show that in some wildfires wind speed can reach U^*_{II}. However, for the largest and longest-heated Particle I, it requires a wind as strong as a typhoon to quench its combustion. Such high critical wind speed is beyond real wildfire scenarios, thus, overheated

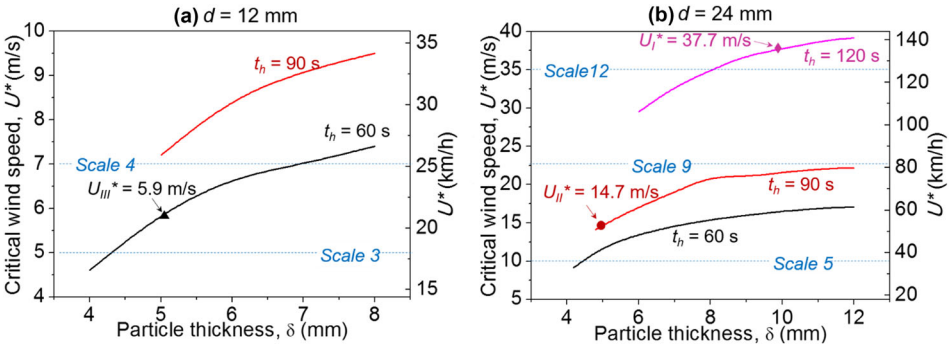

Figure 6. Predicted critical wind speed (U^*) versus particle thicknesses (δ) and heating duration (t_h) for diameter of (a) 12 mm (Particle III), and (b) 24 mm (Particles I and II). The beaufort wind scale [33] is plotted as the reference.

and large particles like Particle III can never be quenched by wind. Due to the limited maximum wind speed from fan (10 m/s), future experiments will be conducted under a more powerful wind tunnel for different particle sizes and heating durations to further verify current theoretical predictions. In addition, the measured distributions of mass loss and transport distance will be used to validate existing analytical and numerical models in the literature.

5. Conclusions

In this study, we experimentally study the burning of three disc firebrands (weighing about 1 g) by measuring the distributions of transport distance and residue mass under two wind speeds of 5 and 7 m/s. For the first time, a bimodal (burning and extinction modes) distribution is found for small firebrands under certain wind speeds (firebrands of 12-mm diameter and 5-mm thickness under a wind speed of 7 m/s in this work). Specifically, the transport distance in the extinction mode is found to be 130 cm, shorter than 200 cm in the burning mode. The proposed heat transfer analysis shows that there is a critical wind speed dividing unimodal and bimodal distributions, above which the firebrands tend to be quenched by the wind cooling. The predicted critical wind speed agrees with experimental measurements. Theoretical analysis further predicts that this critical wind speed increases with both the particle size and the initial heating duration. All these results are expected to be applied in estimating the transport distance of firebrands in prevention of practical spot fires.

Acknowledgements

This research is funded by the National Natural Science Foundation of China (Nos. 51625602 and 51476156) and the National Key Research and Development Plan (No. 2016YFC0800100). This work was also supported by the Fundamental Research Funds for the Central Universities (Nos. WK2320000033 and WK2320000036).

References

1. Johnson EA, Miyanishi K (2001) Forest fires: behavior and ecological effects. Elsevier Science, Amsterdam
2. Mell WE, Manzello SL, Maranghides A, Butry D, Rehm RG (2010) The wildland–urban interface fire problem—current approaches and research needs. Int J Wildland Fire 19(2):238–251. doi:10.1071/WF07131
3. Koo E, Linn RR, Pagni PJ, Edminster CB (2012) Modelling firebrand transport in wildfires using HIGRAD/FIRETEC. Int J Wildland Fire 21(4):396–417. doi:10.1071/WF09146
4. Williams FA (1982) Urban and wildland fire phenomenology. Prog Energy Combust Sci 8(4):317–354. doi:10.1016/0360-1285(82)90004-1

5. Albini FA, Forest I (1979) Spot fire distance from burning trees: a predictive model. Intermountain forest and range experiment station. BForest Service, US Department of Agriculture, Ogden, Utah, USA
6. Ellis PFM (2013) Firebrand characteristics of the stringy bark of messmate (Eucalyptus obliqua) investigated using non-tethered samples. Int J Wildland Fire 22(5):642–651. doi:10.1071/WF12141
7. Pagni PJ (1993) Causes of the 20 october 1991 Oakland hills conflagration. Fire Saf J 21(4):331–339. doi:10.1016/0379-7112(93)90020-Q
8. Caton SE, Hakes RSP, Gorham DJ, Zhou A, Gollner MJ (2016) Review of pathways for building fire spread in the wildland urban interface part I: exposure conditions. Fire Technol. doi:10.1007/s10694-016-0589-z
9. Hakes RSP, Caton SE, Gorham DJ, Gollner MJ (2016) A review of pathways for building fire spread in the wildland urban interface part II: response of components and systems and mitigation strategies in the United States. Fire Technol. doi:10.1007/s10694-016-0601-7
10. Tarifa CS, Notario P, Moreno FG (1965) On the flight paths and lifetimes of burning particles of wood. In: Symposium (international) on combustion, vol 10. Elsevier, pp 1021–1037. doi: 10.1016/S0082-0784(65)80244-2
11. Tarifa C, Del Notario P, Moreno F, Villa A (1967) Transport and combustion of firebrands, final report of grants FG-SP-11 and FG-SP-146. US Department of Agriculture Forest Service, Madrid, Spain
12. Lee S-L, Hellman J (1969) Study of firebrand trajectories in a turbulent swirling natural convection plume. Combust Flame 13(6):645–655. doi:10.1016/0010-2180(69)90072-8
13. Albini FA (1983) Transport of firebrands by line thermals. Combust Sci Technol 32(5–6):277–288. doi:10.1080/00102208308923662
14. Woycheese J, Pagni P (1999) Combustion models for wooden brands. In: Proceedings 3rd international conference on fire research and engineering. Society of fire protection engineers, Washington, USA, 1999. p 53
15. Himoto K, Tanaka T (2005) Transport of disk-shaped firebrands in a turbulent boundary layer. In: The eighth international symposium on fire safety science, pp 18–23
16. Manzello SL, Maranghides A, Mell WE (2007) Firebrand generation from burning vegetation. Int J Wildland Fire 16(4):458–462. doi:10.1071/WF06079
17. Manzello SL, Maranghides A, Shields JR, Mell WE, Hayashi Y, Nii D (2009) Mass and size distribution of firebrands generated from burning Korean pine (Pinus koraiensis) trees. Fire Mater 33(1):21–31. doi:10.1002/fam.977
18. Manzello SL, Shields JR, Cleary TG, Maranghides A, Mell WE, Yang JC, Hayashi Y, Nii D, Kurita T (2008) On the development and characterization of a firebrand generator. Fire Saf J 43(4):258–268. doi:10.1016/j.firesaf.2007.10.001
19. Zhou K, Suzuki S, Manzello SL (2015) Experimental study of firebrand transport. Fire Technol 51(4):785–799. doi:10.1007/s10694-014-0411-8
20. Manzello SL, Suzuki S (2013) Experimentally simulating wind driven firebrand showers in Wildland-Urban Interface (WUI) fires: overview of the NIST firebrand generator (NIST dragon) technology. Procedia Eng 62:91–102. doi:10.1016/j.proeng.2013.08.047
21. Tse SD, Fernandez-Pello AC (1998) On the flight paths of metal particles and embers generated by power lines in high winds—a potential source of wildland fires. Fire Saf J 30(4):333–356. doi:10.1016/S0379-7112(97)00050-7
22. Anthenien RA, Tse SD, Carlos Fernandez-Pello A (2006) On the trajectories of embers initially elevated or lofted by small scale ground fire plumes in high winds. Fire Saf J 41(5):349–363. doi:10.1016/j.firesaf.2006.01.005

23. Sardoy N, Consalvi J-L, Porterie B, Fernandez-Pello AC (2007) Modeling transport and combustion of firebrands from burning trees. Combust Flame 150(3):151–169. doi:10.1016/j.combustflame.2007.04.008
24. Sardoy N, Consalvi J, Kaiss A, Fernandez-Pello A, Porterie B (2008) Numerical study of ground-level distribution of firebrands generated by line fires. Combust Flame 154(3):478–488. doi:10.1016/j.combustflame.2008.05.006
25. Ellis P (2010) The effect of aerodynamic behaviour of flakes of jarrah and karri bark on their potential behaviour as firebrands. J R Soc West Aust 93:21–27
26. Knight I, Ellis P, Sullivan A (2001) The CSIRO vertical wind tunnel. CSIRO forestry and forest products, technical report
27. Knight I (2001) The design and construction of a vertical wind tunnel for the study of untethered firebrands in flight. Fire Technol 37(1):87–100. doi:10.1023/A:1011605719943
28. Tohidi A, Bridges W (2015) Statistical description of firebrand size and shape distribution from coniferous trees for use in Metropolis Monte Carlo simulations of firebrand flight distance. Fire Saf J 77:21–35. doi:10.1016/j.firesaf.2015.07.008
29. Koo E, Pagni PJ, Weise DR, Woycheese JP (2010) Firebrands and spotting ignition in large-scale fires. Int J Wildland Fire 19(7):818–843. doi:10.1071/WF07119
30. Houssami EM, Mueller E, Filkov A, Thomas JC, Skowronski N, Gallagher MR, Clark K, Kremens R, Simeoni A (2016) Experimental procedures characterising firebrand generation in wildland fires. Fire Technol 52(3):731–751. doi:10.1007/s10694-015-0492-z
31. Cheney NP, Gould JS, Catchpole WR (1998) Prediction of fire spread in grasslands. Int J Wildland Fire 8(1):1–13. doi:10.1071/WF9980001
32. Andrews PL, Cruz MG, Rothermel RC (2013) Examination of the wind speed limit function in the Rothermel surface fire spread model. Int J Wildland Fire 22(7):959–969. doi:10.1071/WF12122
33. Beer T (1996) Environmental oceanography. CRC marine science. Taylor & Francis, Routledge
34. Englund F, Nussbaum RM (2000) Monoterpenes in Scots pine and Norway spruce and their emission during kiln drying. Holzforschung 54(5):449–456. doi:10.1515/HF.2000.075
35. Samuelsson R, Nilsson C, Burvall J (2006) Sampling and GC-MS as a method for analysis of volatile organic compounds (VOC) emitted during oven drying of biomass materials. Biomass Bioenergy 30(11):923–928. doi:10.1016/j.biombioe.2006.06.003
36. Song J, Wang S, Chen H (2014) Safety distance for preventing hot particle ignition of building insulation materials. Theor Appl Mech Lett 4(3):034005. doi:10.1063/2.1403405
37. Bergman TL, Incropera FP (2011) Introduction to heat transfer. Wiley, Hoboken
38. Su Y, Luo Y, Wu W, Zhang Y, Zhao S (2012) Characteristics of pine wood oxidative pyrolysis: degradation behavior, carbon oxide production and heat properties. J Anal Appl Pyrolysis 98:137–143. doi:10.1016/j.jaap.2012.07.005
39. Bergman TL, Incropera FP, Lavine AS (2011) Fundamentals of heat and mass transfer. Wiley, Hoboken
40. Di Blasi C (1994) Processes of flames spreading over the surface of charring fuels: effects of the solid thickness. Combust Flame 97(2):225–239. doi:10.1016/0010-2180(94)90006-X
41. Grishin AM (1997) Mathematical modeling of forest fires and new methods of fighting them. Publishing House of the Tomsk state university, Siberia, Russia
42. Quintiere JG (2006) Fundamentals of fire phenomena. Wiley, Hoboken